Growth temperature dependence of magnetoresistance in Co/Cu(111) wedged superlattices

G. R. Harp, S. S. P. Parkin, R. F. C. Farrow, R. F. Marks, M. F. Toney, Q. H. Lam, T. A. Rabedeau, and R. J. Savoy
IBM Almaden Research Center, 650 Harry Road, San Jose, California 95120-6099
(Received 25 November 1992)

The relationship of the growth and structure of highly oriented (111) Co/Cu superlattices to their magnetotransport properties is discussed. To eliminate changes in growth parameters between different samples, wedged superlattice structures were prepared in which uniform Co layers are separated by Cu layers whose thickness is varied by more than a factor of 2 across the substrate. Smooth variations in magnetoresistance (MR) as a function of Cu-layer thickness were obtained. No evidence for oscillations in MR was found with the exception of a peak in MR for thin Cu layers centered at about 10 Å. The magnitude of the MR at this peak was found to increase substantially for growth at 150 °C relative to growth at 0 °C. The increased MR is correlated with smoother Co/Cu interfaces as determined from *in situ* x-ray-photoelectron-diffraction studies and *ex situ* x-ray-diffraction experiments. At 150 °C it is found that Cu has a tendency to surface segregate at all stages during growth. Studies of the growth of Cu on Co show the presence of Co near (but excluded from) the surface even after the growth of relatively thick Cu layers. At both 0 °C and 150 °C, the superlattices showed a relatively high degree of surface roughness, when compared with the Cu and Co layer thicknesses. Either of these results suggest a mechanism for ferromagnetic bridging of the Co layers, previously conjectured to play an important role in (111) Co/Cu superlattices.

I. INTRODUCTION

In the past several years, novel magnetic and electronic properties have been discovered in ferromagnetic and nonmagnetic metallic multilayer systems, including giant magnetoresistance,[1–5] and oscillatory interlayer magnetic exchange coupling.[3,4,6] In the latter effect, the exchange coupling between neighboring ferromagnetic layers oscillates between ferromagnetic and antiferromagnetic (AF) coupling as a function of the nonmagnetic spacer layer thickness. The Co/Cu multilayer system has shown record values of magnetoresistance. The saturation magnetoresistance (MR) is defined as the difference (ΔR) between the peak resistivity and the resistivity at high external field divided by the resistivity at high field (R). In Co/Cu multilayers, this MR can exceed 65% at room temperature and 120% at 4.2 K.[4,5]

The Co/Cu system has been extensively investigated both in multilayers and sandwiches using a variety of growth techniques. Recently the twin discoveries of oscillatory interlayer magnetic coupling[5] and giant MR (Refs. 5 and 6) in sputtered Co/Cu multilayers has renewed interest in this system. For sputtered multilayers, it was found that the use of an Fe buffer layer[5] was essential to obtain the maximum degree of antiferromagnetic coupling of the Co layers, since it gives rise to very flat Co and Cu layers. While it might have been expected that molecular-beam epitaxy (MBE) growth techniques would lead to higher-quality Co/Cu superlattice (SL) structures, it was a surprise when several groups using MBE found no evidence for antiferromagnetic coupling in Co/Cu[111] oriented SL's,[7,8,9] although AF coupling and oscillations in AF coupling were reported in [100] (Refs. 10–14)- and [110] (Ref. 15)- oriented Co/Cu SL's or sandwiches. Recently, however, evidence for AF coupling in (111)-oriented Co/Cu has been reported by several groups,[16–19,15] at least for very thin Cu layers. For thicker Cu layers, the magnetic behavior has not been sufficiently explored to determine whether or not oscillations in the AF coupling exist. Measurements of such coupling in the [111] orientation are complicated by the apparent presence of defects which result in ferromagnetic coupling of the magnetic layers. These defects seem to be extremely sensitive to the growth procedures used, and even samples which appear nearly identical can have very different MR characteristics.[19]

In this paper we study the growth of Co/Cu wedge multilayered structures on specially prepared pre-scribed sapphire wafers. The relationship of growth of these structures as a function of deposition temperature to their magnetotransport properties is discussed. Detailed investigations of the structure of individual Co and Cu layers are presented using x-ray-photoelectron diffraction and spectroscopy, and x-ray reflectivity. These studies elucidate the origin of ferromagnetic bridges between neighboring Co layers, probably resulting from large interlayer roughness or diffusion of Co along grain boundaries within the Cu layers.

II. EXPERIMENT

The substrates for film growth are rectangular basal-plane sapphire strips (Insaco), with dimensions of approximately $56\times11\times0.5$ mm^3. The back sides of the substrates are scribed to a depth of 0.25 mm at 2 mm intervals across the along the length of the strip. After growth of the superlattice, these strips can be easily broken into 28 2×11 mm^2 pieces for measurement of magnetoresistance.

The SL's are prepared in a VG-80M system with a base

pressure of 4×10^{-11} mbar. Electron gun sources are used for the deposition of Pt and Co films, and an effusion cell is used for the deposition of Cu. Growth rates in the range of 0.1–0.25 Å/s are typically used. Epitaxy with the sapphire substrate is achieved with the growth of a 60 Å Pt buffer layer at 600 °C, which grows in the [111] orientation.[20] The platinum crystallites can form in two orientations on the sapphire, azimuthally oriented 180° apart. This gives rise to very sharp sixfold low-energy electron-diffraction (LEED) and reflection high-energy electron-diffraction (RHEED) patterns. X-ray structural studies of such platinum films show that they have an average crystalline domain (grain) size of $\simeq$200 Å, and a texture axis has a dispersion of only 0.5° full width at half maximum (FWHM).[20]

The Co/Cu SL's are then deposited on the Pt buffer layer, beginning and ending with Co, including 31 Co layers and 30 Cu layers. Finally, a 30 Å Pt capping layer is deposited to prevent sample oxidation, giving an overall structure of Pt (30 Å)/Co(8 Å)/[Cu(x)Co(8 Å)]$_{30}$/Pt(60 Å)/ sapphire (0001). All of the SL's and structures discussed here show good crystalline ordering, as determined by RHEED and LEED. The Co/Cu [111] texture axis for these samples had a dispersion of 0.5° FWHM.[19] After the initial Pt buffer layer, deposition is performed at 0, 150, or 200 °C substrate temperature. The photoelectron and x-ray reflectivity measurements are made at room temperature, and MR is measured both at room temperature and at $\simeq$4.2 K.

The thickness variation of the Cu spacer layers is obtained by orienting the effusion cell at about 30° to the sample surface normal direction, with a sample-to-source distance of about 30 cm. This gives rise to a copper deposition rate which varies by more than a factor of 2 over a 2-in. sample, as demonstrated in Fig. 1. Here the Cu thickness is plotted as a function of sample position for a deposition made onto a glass slide. The Cu thickness is measured by ellipsometry. The polynomial fit of the Cu thickness, t (Å), versus sample position, x (mm), shows a high degree of linearity (see Fig. 1).

X-ray-photoelectron-diffraction (XPD) and x-ray-photoelectron-spectroscopy (XPS) measurements are made in a VG Microlab-II system. Samples are transferred from the deposition chamber to the electron spectroscopy for chemical analysis (ESCA) lab in ultrahigh vacuum (UHV) ($<10^{-10}$ mbar). XPD is performed on samples specially prepared for this purpose on 1-in. sapphire, initially having the structure Co(x)/Cu(100 Å)/Co(20 Å)/Pt(60 Å)/ sapphire (0001). After an XPD measurement is made, the next sample is prepared by the subsequent growth of Cu(100 Å) and then another thin Co layer. Thickness calibrations for these films are derived by XPS measurements of the intensity of the Co and Cu $2p_{3/2}$ photoemission lines, as compared with standards.

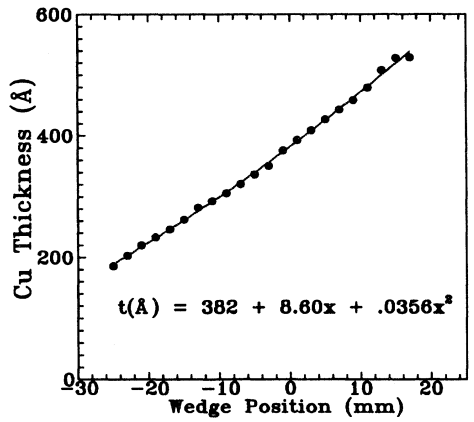

FIG. 1. Thickness of a wedged Cu film on glass as measured by ellipsometry. Note that the variation of Cu-layer thickness with position on the sample is very linear.

All photoelectron measurements were made using Mg K_α incident x-radiation. The XPD measured the Co $2p$ photoemission line, including both the $\frac{3}{2}$ and $\frac{1}{2}$ spin-orbit components. Plotted XPD intensities are the integrated signal of this photoemission peak as a function of polar angle after the subtraction of a linear background. No attempt is made to normalize this intensity to a background function, since for such thin layers this background function is difficult to determine experimentally. This presents no difficulty, as the XPD features of interest are clearly evident in the raw data.

The resistance of the samples was measured using a low-frequency ac technique with a conventional four-in-line contact geometry. The contacts were made with gold-plated spring-loaded pressure contacts. The current was in the plane of the sample and the field was aligned either in the plane of the sample, parallel or orthogonal to the current, or perpendicular to the plane of the sample.

The x-ray reflectivity experiments were conducted using radiation from an 18 kW x-ray generator operating with a line focus. A flat Ge(111) crystal was used to select the Cu K_{α_1} line. The spot size at the sample was defined by slits just before the sample and was approximately 0.15 by 2.5 mm in and out of the scattering plane, respectively. The angular acceptance of the detector was also defined by slits and was 2 milliradian (mrad) in the scattering plane and 19 mrad out of the scattering plane. The large acceptance out of the scattering plane effectively integrates the diffuse x-ray scattering (from the multilayer roughness) in this direction.

Low-angle x-ray reflectivity was measured on samples specially prepared for this purpose on 1-in. diameter sapphire wafers. The samples have nominally the same structure as the superlattice wedges except that the platinum buffer layer was only 30 Å thick, and the samples had a uniform Cu spacer layer thickness of $\simeq$10 Å. The two samples were deposited in consecutive runs to minimize the drift of deposition rate of the sources. The miscut in the sapphire substrates is $\simeq$0.5°, and the resulting steps in the substrates cause an azimuthal dependence to the diffuse x-ray scattering. The direction of the miscut (and the steps) was aligned out of the scattering plane.

III. MAGNETORESISTANCE AND MAGNETIZATION

Several Co/Cu(111) wedges were grown at a substrate temperature of 0 °C. The Co layer thickness, was $\simeq8\pm1$

Å in each of the wedges. The Cu layer thickness, t_{Cu}, varied by approximately a factor of 2 along each wedge, as mentioned above. Typical resistance versus in-plane orthogonal field are shown in Fig. 2 for two samples with $t_{Cu}=10.8$ and 67 Å. Data are included for measurements at both 4.2 and 290 K.

For the sample with $t_{Cu}=10.8$ Å, the MR is only weakly dependent on temperature [MR(4.2 K)/MR(290 K) $\simeq 1.2$] whereas for $t_{Cu}=67$ Å, the MR increases strongly with decreasing temperature [MR(4.2 K)/MR(290 K) $\simeq 4.2$]. This may be partly due to shunting through the Pt layers in the structure.[19] Note that the wedges are grown on a buffer layer of Pt 60 Å thick and with a Pt capping layer 30 Å thick. Since the conductivity of the Pt layer increases significantly with decreasing temperature, the shunting of current through the Pt layers will increase at lower temperatures, tending to reduce the MR. This shunting effect will be greatest for thin Cu layers. In the limit of thick copper layers, the effect of shunting through the Pt will become negligible.

Four wedges with overlapping Cu thickness ranges were used to span Cu thicknesses between 6 and 75 Å. The saturation magnetoresistance values measured at 4.2 K and 290 K for these samples are plotted in Fig. 3(a) as a function of Cu layer thickness. Each of the four different symbols in the figure corresponds to a series of measurements made on different parts of a given wedge. Note that the data overlap well from wedge to wedge indicating good reproducibility from deposition to deposition. Within a series, the MR varies smoothly with Cu layer thickness, especially when compared with data on individually prepared Co/Cu(111) samples.[19] Day-to-day variations in deposition conditions are probably responsible for the variability of the MR in individually prepared samples. But with the wedged superlattice technique, such uncontrolled variations can be suppressed.

It is seen that the MR shows a single maximum, near 10 Å, for deposition at 0 °C. At room temperature, the MR then decreases to $\simeq$ 7% for $t_{Cu}=15$ Å, and then remains constant, up to $t_{Cu}\sim 75$ Å. The 4.2 K measurements show the same MR maximum near 10 Å, and then above $t_{Cu}\sim 16$ Å, a monotonically increasing MR with increasing t_{Cu}. At $t_{Cu}=75$ Å the MR is 30%, nearly equal to the peak MR at $t_{Cu}=10$ Å. The increasing divergence of the MR at the two temperatures may be partly ascribed to the decreasing influence of the Pt buffer layers with increasing t_{Cu}, as discussed above. But the fact that the MR at both room temperature and 4.2 K shows only a monotonic behavior with larger values of t_{Cu} is rather surprising, since similar (polycrystalline) structures deposited by dc magnetron sputtering show oscillatory MR.[5] Such sputtered samples display up to four peaks in MR with increasing t_{Cu}, with a period of $\simeq 10-11$ Å. Furthermore, the amplitude of the first MR maximum in these wedges is less than half as large as that obtained for sputtered samples.[5]

This latter result is due to incomplete antiferromagnetic alignment in the MBE deposited samples. Apparently, some regions of the MBE samples are magnetically bridged (ferromagnetically coupled), even for Cu thicknesses corresponding to the AF coupling peak. Thus, only a fraction of the sample contributes to the MR signal (see Ref. 19). But the absence of the MR peaks at higher Cu-layer thickness remains a dilemma.

It is interesting to note that very large fields are required to saturate the MR for all these samples, as compared with sputtered films, where the saturation field is much lower. However the shape of the resistance versus field curves can vary with t_{Cu}, as shown in Fig. 2. For thin Cu layers the bell shape of the MR curves is similar to those found in strongly antiferromagnetically coupled structures prepared by magnetron sputtering. For thicker Cu layers the shape of the resistance versus field curves is distinctly different, showing a sharp peak near zero field. We find that for $t_{Cu} \gtrsim 15$ Å this shape becomes ap-

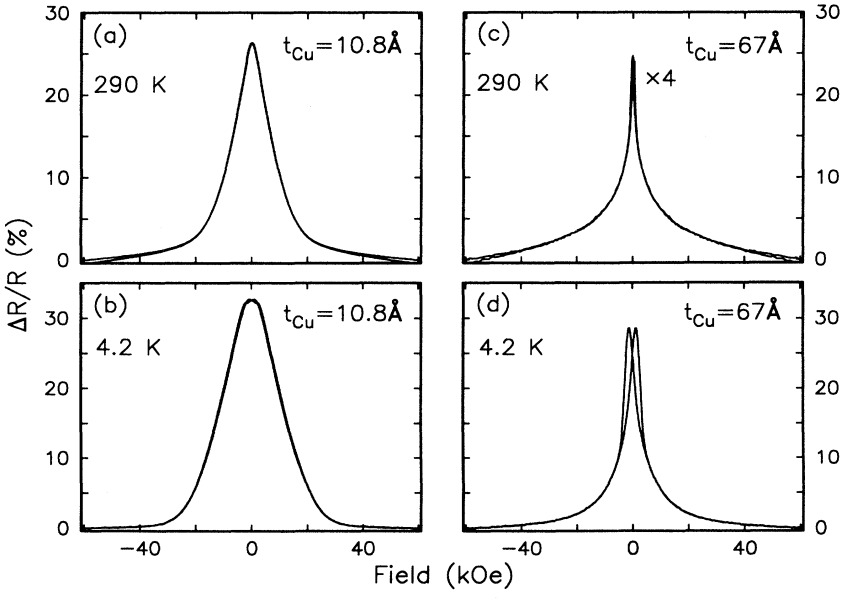

FIG. 2. Magnetoresistance vs applied field for two superlattices deposited at 0 °C. Figs. (a) and (b) are the room temperature and $\simeq$4.2 K MR measurements from a superlattice having Cu layers 10.8 Å thick, (c) and (d) are the analogous measurements made on a superlattice having Cu layers 67 Å thick.

proximately independent of Cu-layer thickness.

Several wedges were prepared at higher deposition temperatures of 150 and 200 °C. MR values as a function of Cu layer thickness for two wedges prepared at 150 °C are shown in Fig. 3(b). As for 0 °C deposition, only a single MR peak is observed at $\simeq 10$ Å, after which the MR varies smoothly, showing no oscillatory behavior. The 4.2-K MR values diverge smoothly from the room-temperature measurements for increasing t_{Cu} (again partly because of current shunting by the Pt). Deposition at 200 °C showed very similar results as for epitaxy at 150 °C. In particular, no additional peaks in MR were observed beyond the initial peak at $\simeq 10$ Å with increasing t_{Cu}.

However, the MR of samples deposited at 150 °C do show significant differences as compared with the MR of samples deposited at 0 °C. First, the peak value of MR for $t_{Cu} \simeq 10$ Å is about 25% higher for deposition at 150 °C than for deposition at 0 °C. Second, above $t_{Cu} \simeq 15$ Å, the 4.2-K MR increases with increasing t_{Cu} for 0 °C deposited samples, whereas for 150 °C samples the 4.2-K MR is nearly constant. This leads to an inverted situation where there is 25% greater MR for the 0 °C sample relative to the 150 °C sample, at $t_{Cu} = 30$ Å.

One might speculate that the enhanced MR at 150 °C for $t_{Cu} \simeq 10$ Å is due to an increase of the AF coupled component (versus the ferromagnetically coupled component) for this growth temperature. To determine whether this is the case, magnetization measurements (using alternating gradient magnetometry) were performed on samples deposited at 0 and 150 °C having t_{Cu} corresponding to the MR peak. The applied magnetic field for these measurements was perpendicular to the plane of the film. This field orientation was chosen because these samples were found to have perpendicular magnetic anisotropy (see below).

The magnetization loops for these two samples are displayed in Fig. 4 and show great similarity. Each loop shows a steeply sloped curve for applied fields $\lesssim 2$ kOe. Above $\simeq 2$ kOe, the slope decreases rapidly, but remains finite even up to large applied fields. Based on comparisons with MR versus field curves, we infer that regions of the sample which become magnetized in low fields, $\lesssim 2$ kOe, are ferromagnetically coupled, and do not contribute to the MR effect. Regions of the sample which magnetize only with large applied fields are AF coupled, and cause the observed changes in MR. The fact that the two magnetization loops look so similar indicates that the ratio of AF coupled to ferromagnetically coupled regions is nearly identical for the two growth temperatures.

As for samples deposited at 0 °C, the saturation field of the 150 °C samples is practically constant above $t_{Cu} = 15$ Å. As the Cu-layer thickness is reduced below 15 Å the saturation field progressively increases, attaining values exceeding 60 kOe for $t_{Cu} = 6.8$ Å, the thinnest Cu layer examined in these studies. This is illustrated in Fig. 5(a) which displays resistance versus field curves for a series of samples deposited at 150 °C with t_{Cu} ranging from 6.8 to 15.7 Å. Note that the saturation field increases monotonically as t_{Cu} is reduced, in contrast with the MR, which peaks at $t_{Cu} \simeq 10$ Å.

These saturation fields are much larger than for comparable structures prepared by dc magnetron sputtering,[4,5] in which both the saturation field and MR show a maximum near $t_{Cu} = 10$ Å. Another important difference between the UHV deposited samples here and the sput-

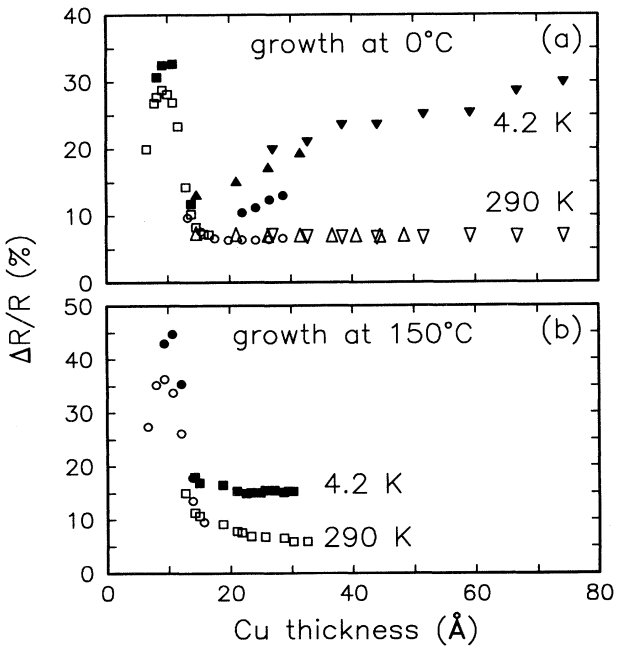

FIG. 3. Magnetoresistance at room temperature (open symbols) and 4.2 K (filled symbols) for samples deposited at 0 °C (a) and 150 °C (b). Data are displayed from total of six wedge samples, with data from a single wedge plotted using the same symbol. The maximum applied field for each measurement was 60 kOe. In all cases, only a single MR peak is observed, near 10 Å. For Cu thicknesses greater than 15 Å, the variation of the MR is monotonic with Cu-layer thickness for all samples, and displays no further MR maxima.

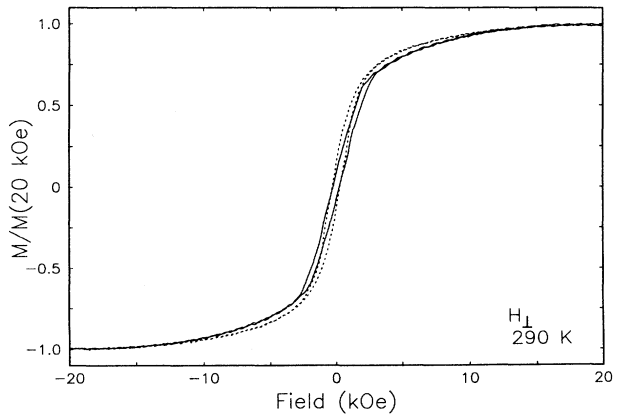

FIG. 4. Magnetization of two samples deposited at 0 °C (solid line) and 150 °C (dotted line), both having t_{Cu} corresponding to the first MR peak. The two curves look very similar, indicating similar ratios of AF coupled to ferromagnetically coupled components in each sample.

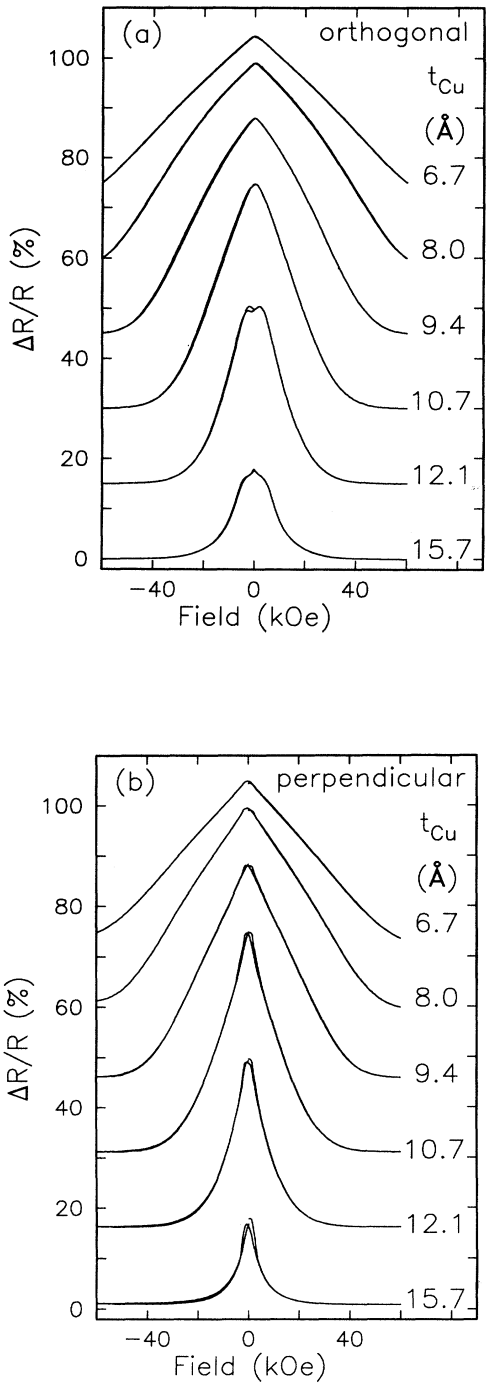

FIG. 5. Magnetoresistance vs field at 4.2 K for samples deposited at 150 °C, with the applied field (a) in the film plane and orthogonal to the sensing current, and (b) perpendicular to the film plane. Note that in graph (a), the saturation field for $t_{Cu}=6.7$ Å exceeds 60 kOe. This saturation field decreases to $\gtrsim$ 20 kOe for $t_{Cu}=15.7$ Å. It was observed that further increase of t_{Cu} did not result in a further decrease of the saturation field. With the applied field perpendicular to the film plane in graph (b), the saturation field of every sample is reduced relative to the in-plane curves of graph (a). This indicates a perpendicular magnetic anisotropy in these superlattices.

tered samples of previous studies[5] is that here we find a strong perpendicular magnetic anisotropy. This is illustrated in Fig. 5(b), where resistance versus field curves at 4.2 K are compared on the same samples as in Fig. 5(a) only with the applied field now perpendicular to the plane of the films. In each case the resistance is saturated in smaller fields for the perpendicular geometry. Such perpendicular anisotropy is present for all Cu-layer thicknesses, and at all growth temperatures.

Although these saturation fields are much larger than those observed in sputtered multilayers,[5] the UHV deposited and sputtered multilayers are similar in that the saturation fields have a very weak temperature dependence. This is illustrated in Fig. 6 where the room-temperature MR is plotted as a function of in-plane applied field, with the field orthogonal to the sensing current, for the same samples as in Fig. 5. It is seen that the saturation field varies by no more than $\simeq 10\%$ between 4.2 K and room temperature.

Magnetor resistance versus field curves for field in-plane and field perpendicular to the plane are shown in Fig. 7 for a 150 °C sample with $t_{Cu}=30$ Å. This figure compares these data with corresponding magnetization loops [as measured by superconducting quantum interference device (SQUID) magnetometry] for the two field orientations. These data demonstrate even more clearly the presence of significant perpendicular magnetic anisotropy. Neither the resistance nor the magnetization of the sample is saturated even for fields as high as 60 kOe. The magnitude of the magnetization at 60 kOe corresponds to

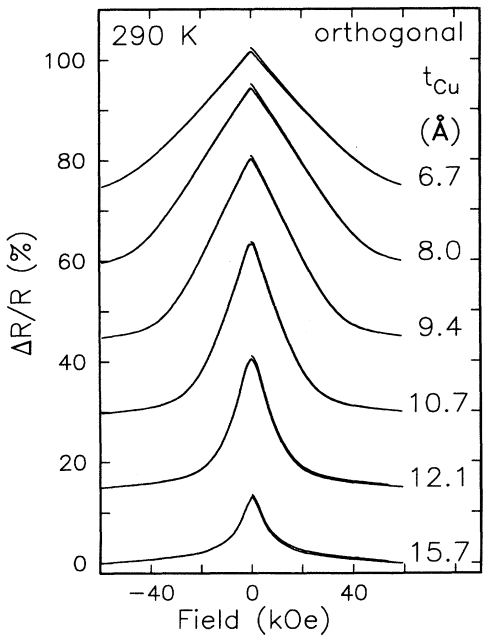

FIG. 6. Magnetoresistance vs field at room temperature for the samples of the previous figure, with the applied field in the film plane and orthogonal to the sensing current. The saturation fields at room temperature are little changed compared with the low-temperature measurements in the same magnetic-field orientation.

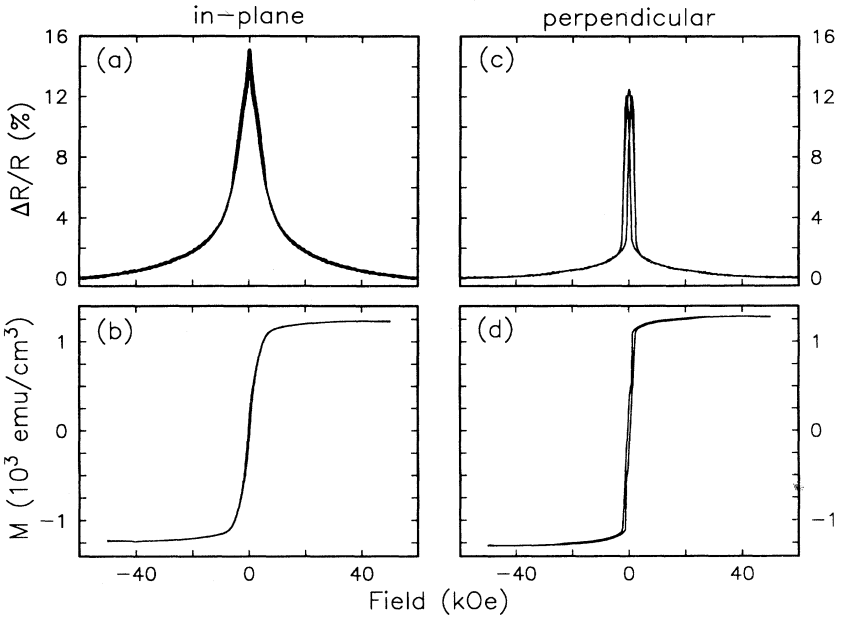

FIG. 7. Magnetoresistance and magnetization vs field at 4.2 K for a sample with $t_{Cu} \simeq 30$ Å deposited at 150 °C. In (a) and (c), the magnetoresistance vs field curves are displayed for the applied field in the film plane, and perpendicular to the field plane, respectively. Curves (b) and (d) show the associated magnetization vs field curves for the same magnetic-field orientations.

approximately 1250 emu/cm^3 (normalized to the volume of Co present in the sample). However, due to the incomplete saturation of these samples, systematic errors in the measurement of Co thickness and volume, and in normalization of the magnetization, this value cannot be distinguished from that of bulk Co (1422 emu/cm^3), within experimental error.

IV. X-RAY REFLECTIVITY

Figure 8 shows the x-ray reflectivity for the SL's grown at 0 and 150 °C. Figure 8(a) contains the specular data or $\theta/2\theta$ scans obtained in a symmetric geometry; here the scattering vector is normal to the optical surface of the substrate.[21] Figure 8(b) contains the off-specular data or $\theta/2\theta$ scans taken with θ offset from the specular condition by 0.34° [i.e., $\theta=(2\theta)/2\pm0.34$].[22] In this case, the scattering vector has a small component parallel to the substrate surface. There are several features in these spectra worthy of note. In the specular scans, one sees the superposition of two oscillations, one with a short period of about 0.011 Å^{-1}, and one with a much longer period of 0.12 Å^{-1}. The longer period is due to the platinum buffer layer, and will not be considered here.

The short-period oscillation results from the interference of x rays reflected from the substrate-metal interface with those reflected from the metal-air interface. Since before growth the substrate is quite smooth, the strength of such oscillations indicates the roughness of the metal-air interface. For the sample grown at 0 °C, these oscillations are weak, and die out quickly with increasing Q_z, the component of the scattering vector perpendicular to the surface. On the other hand, for the 150 °C sample, the oscillations are strong, and persist to larger Q_z. From this we can infer that the metal-air interface of the 0 °C sample is much rougher than of the 150 °C sample. More quantitatively, dynamical modeling of the scattering from these films[23] indicates a root-mean-square (rms) roughness of approximately 20 Å for the 0 °C sample and 8 Å for the 150 °C sample. The overall significance of this roughness will depend on the lateral length scale over which it is distributed, and about which we have little information.

One feature that is surprisingly absent in the spectra of Fig. 8(a) are Bragg peaks due to x-ray scattering from the Co/Cu superlattice. The intensity of these peaks is approximately proportional to the difference in the electron densities of Cu and Co, and since this is small, the Bragg peak intensities are weak. On the other hand, the substrate-metal interface is quite smooth (rms roughness of $\lesssim 2$ Å) as is the surface of the Pt buffer layer.[20] Both

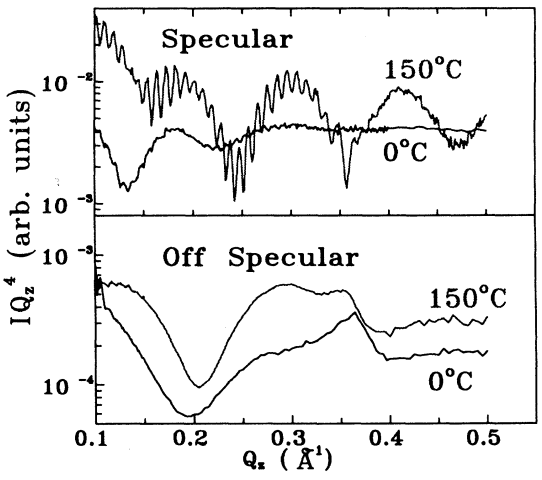

FIG. 8. Low-angle x-ray reflectivity of two samples deposited at 0 and 150 °C. Both have a Cu-layer thickness corresponding to the first MR maximum at about 10 Å. Spectra are for (a) specular reflectivity, and (b) off-specular reflectivity for each sample.

of these interfaces have a large gradient in electron density, giving rise to a large specular x-ray reflectivity. Consequently, the superlattice Bragg peaks are overwhelmed in the specular x-ray reflectivity. It is necessary to go away from the specular scattering geometry to see evidence of the superlattice peaks. The off-specular geometry does not contain the strong specular reflectivity of the Pt interfaces, which enhances the relative amplitude of the superlattice structures. As Fig. 8(b) shows, one superlattice feature is present in both spectra at about 0.36 $Å^{-1}$; we were unable to observe any higher-order peaks due to the low contrast between Co and Cu. The observation of the Co/Cu SL Bragg peak in the *off-specular* reflectivity is due to conformal roughness in the SL.[24]

From these spectra we begin to understand why 150 °C growth shows improved MR in these SL's. In the absence of interdiffusion, the metal-air interface reflects the quality of the internal Co/Cu interfaces. Smoother interior interfaces for 150 °C growth could account for higher MR at $t_{Cu} = 10$ Å.

V. X-RAY-PHOTOELECTRON DIFFRACTION

The surface free energy of Cu is lower than that of Co (1.9 J/m^2 versus 2.7 J/m^2,[25] respectively) and therefore it is expected that Cu will grow in a uniform layer-by-layer fashion on Co over a wide range of temperatures. Because Co and Cu are largely immiscible below 400 °C,[26] one expects relatively little bulk interdiffusion at the Co-Cu interfaces. However, the growth of a uniform Co layer on a Cu surface presents a problem since this is not a thermodynamically stable situation. We might expect, at moderate temperatures, that Co deposited on Cu might form three-dimensional islands, or that Cu atoms will diffuse to the surface of the Co layer to reduce the surface free energy. Auger peak height ratio measurements[27] indicate that some Co-Cu interdiffusion begins to occur in the (111) orientation above 150 °C, although the nature of this interdiffusion is not known.

To study the initial growth behavior of Co/Cu(111) we use x-ray-photoelectron diffraction.[28] XPD possesses unique capability for the measurement of growth behavior because, unlike x-ray reflectivity, XPD does not rely on differential electron densities to interrogate the structure. Instead, XPD achieves chemical sensitivity by detecting electrons which originate only from atoms of one chemical species. In this way, XPD determines the placement of specific atomic types in the growing structure.

At electron kinetic energies exceeding 500 eV, the photoelectron intensity peaks along internuclear directions (atomic chains) in the sample. That is, if there is any atom between the electron emitter and the detector, that scattering atom will give rise to a photoelectron peak at the angle corresponding to the internuclear axis of the emitter and scatterer. Thus, XPD can readily determine whether or not the initial stages of heteroepitaxy are layer by layer. For example, if a single monolayer of Co is deposited on a Cu surface, then layer-by-layer growth gives rise to a nearly isotropic XPD intensity for emission from the Co atoms. However, if Co islanding or Cu surface segregation occurs, then peaks will appear in the XPD at specific angles, according to the crystal structure.

The atomic geometry of Co/Cu(111) is depicted schematically in Fig. 9. Here, we consider photoelectron emitters in the first, second, third, and fourth layers of an fcc(111) single crystal. The figure corresponds to a section through the crystal perpendicular to the surface and corresponding to the $[1\bar{1}0]$ scattering plane. If a Co atom exists in the outermost layer of this crystal, then its XPD intensity will vary smoothly as a function of angle, except near grazing exit angles. A Co atom in the second layer will present XPD peaks at $+35.3°$ and $-54.7°$, as measured from surface normal. A Co atom in the third layer will possess these peaks, plus additional (weaker) peaks at $-19.5°$ and 60.5°. Finally, an atom in the fourth layer possesses all these peaks, but also displays a peak at normal emission. Thus, by noting the presence or absence of these peaks in the XPD intensity, we can estimate the population of Co atoms in each of these four emitting depths. In this report, we will concentrate only on the peaks at 35° and 54° (second layer), and at 0° (fourth layer), since these are the strongest, and therefore most easily detectable features in this diffraction plane. Because of 180° twinning for Pt expitaxy on sapphire, the XPD intensity in this scattering plane is effectively mirrored about normal emission. Therefore, with a single polar angle scan from 0° to 70°, it is possible to probe the XPD intensity of the three major features at 0°, 35°, and 55°.

Figure 10 presents the Co photoemission intensity as a function of polar angle, from thin Co films on thick Cu deposited at 0 °C. Films were prepared with thicknesses of 0.8, 1.5, 2.3, and 3 equivalent monolayers (ML). Note that all these spectra show a precipitous drop in photoemission intensity at angles greater than 60°. This drop is due to geometrical factors inherent in our measurement apparatus, such as the decreasing solid angle subtended by the sample as viewed by the electron detector. The drop is present in all the XPD data we present here, and does not relate to the problem at hand.

The XPD intensity for the 0.8 ML film shows a nearly isotropic angular distribution, as seen in Fig. 10. This indicates a nearly layer-by-layer growth mode for this film. Perhaps a very weak intensity is observed for the 35° and

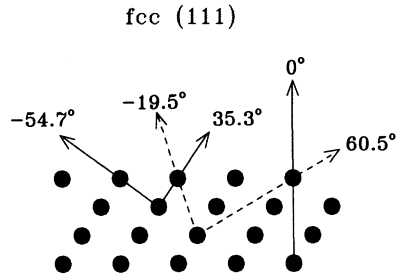

FIG. 9. Diagram of atoms near an fcc(111) surface, in the $[1\bar{1}0]$ scattering plane. The strongest XPD features are found at 35.3°, 54.7°, and normal emission (0°). Weaker features can be seen in very thick films at 19.5° and 60.5°.

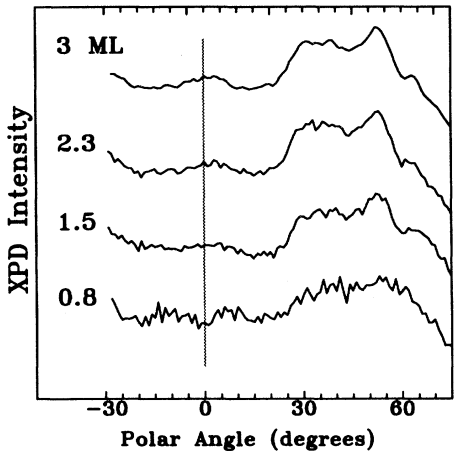

FIG. 10. XPD polar angle scans from thin Co films grown on thick Cu at 0 °C. The integrated intensity of the Co 2*p* peaks are plotted. For 0.8 ML Co, the intensity shows little evidence for the second-layer peaks at 35° and 55°, indicating nearly layer-by-layer growth. Similarly, at 3.0 ML, the fourth-layer normal emission peak is very weak, also indicating nearly monolayer growth.

55° peaks, indicating Co atoms in the second layer from the surface. This is consistent with diffusion-limited growth, where Co atoms arriving at monolayer Co islands do not always diffuse to the island edges, but sometimes form small second layer clusters before the first monolayer is complete.

In contrast with the 0.8 ML film, the 1.5 ML film shows strong diffraction features at 35° and 55° polar angles. Thus, a significant number of Co atoms reside in the second layer from the surface. This is expected, since for 1.5 ML, at least 0.5 ML of the Co atoms resides in the second layer. At 2.3 and 3.0 ML, the peaks at 35° and 55° do not significantly change in their appearance. This too is to be expected, since the associated atomic chains for these features exist for all atoms below the surface layer.

More information about the growth mode can be found by examining the XPD intensity near normal emission. No significant feature is seen at this position until the Co layer reaches 3.0 ML thickness, where a weak feature begins to appear. Again, this behavior implies nearly layer-by-layer growth, since no Co atoms reside in the fourth layer until three layers are nearly complete. The presence of a weak feature at 3.0 ML is again consistent with diffusion-limited growth, which would cause the formation of small fourth-layer terraces before the completion of the third layer. We therefore conclude from the XPD measurements that at 0 °C, Co grows on Cu(111) in a nearly layer-by-layer mode, without a large amount of Co-Cu interdiffusion.

The XPD results at 150 °C, however, reveal a very different story about the growth mode. These data are shown in Fig. 11. Here, for 0.8 ML equivalent thickness, the Co film already shows strong 35° and 55° XPD features. Thus, a large fraction of the deposited Co atoms must be emitting from *beneath* the surface. In principle, this could be due either to Co islanding or to the surface segregation of Cu. At higher Co film thicknesses, the 35° and 55° peaks do not change significantly.

Examining the spectra near normal emission, we find that a significant peak begins to develop when the film thickness exceeds 2 ML. At 3.0 ML, this peak is already relatively strong, signifying Co atoms in the fourth layer. Once again, this could be due either to Co islanding or to the surface segregation of Cu.

It would be useful to distinguish between the two possible growth modes at 150 °C. Based on the XPD data alone, we have a hint from the thicknesses at which different peaks arise. Specifically, when about 1 ML of Co is deposited, the XPD sees many Co atoms in the second layer. When 3 ML is deposited, many Co atoms are seen in the fourth-layer position, but few fourth-layer atoms are seen for 2.3 ML, and none for 1.5 ML. It would therefore appear that at all Co-layer thicknesses, there is just one extra monolayer of atoms at the surface. This is consistent with the presence of a floating Cu monolayer, which constantly surface segregates during Co film growth. One would expect that Co islanding would not lead to just one additional monolayer, but rather that the fourth-layer peak would already begin to appear for depositions below 2 ML.

The floating Cu monolayer model is consistent with the X-ray reflectivity. If the Co films showed strong islanding at 150 °C relative to 0 °C, then one would expect a rougher vacuum interface with higher-temperature growth. On the other hand, a floating Cu monolayer could lead to a smoother surface morphology, particularly if the Cu acted as a surfactant for the growth process. Such surfactant behavior is seen in some semiconductor systems[29,30] and in the Fe-Au system.[31,32] At the same time, Cu surface segregation has been observed for Co films deposited on Cu(100) (Refs. 33 and 34) at temperatures as low as 177 °C, which is close to our deposition temperature. Therefore, we conclude that the model of surface segregated Cu agrees best with the observed data.

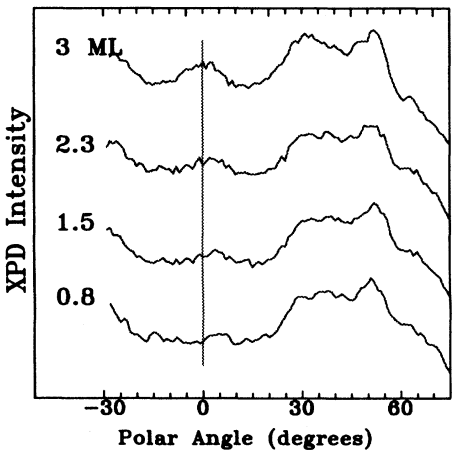

FIG. 11. Same as previous figure except that the films were deposited at 150 °C. Unlike the depositions at 0 °C, at 0.8 ML, the second-layer peaks at 35° and 55° are already strong. Similarly, at 3.0 ML, the fourth-layer peak at normal emission is strong. These data indicate the surface segregation of Cu.

VI. X-RAY-PHOTOELECTRON SPECTROSCOPY

To further test these models of the growth modes, and to probe the regime of thicker layers, x-ray-photoelectron spectroscopy was performed on samples prepared with very thick ($\simeq$100 Å) Co and Cu layers. Such layers are thick enough that only the most recent deposition should contribute to the XPS signal, unless there are significant interdiffusion or surface segregation effects.

Beginning with 0 °C deposition, a sample was prepared with 100 Å Cu deposited onto 100 Å Co. As with all samples discussed in this section, this film showed excellent crystalline ordering, as determined by LEED and XPD. The XPS spectrum for this sample at normal emission is displayed in Fig. 12(a). This spectrum shows the features corresponding to Cu (such as the Cu *LVV* Auger peak) but shows no feature corresponding to Co (e.g., the Co *LMM* Auger peak). On top of this Cu film, another 100 Å of Co was then deposited at 0 °C. The XPS spectrum from this sample is displayed in Fig. 12(b). Here, strong features appear corresponding to the Co film, but no evidence of Cu spectral features are seen. These results are consistent with the interpretation that there is no interdiffusion between the Co and Cu at 0 °C.

At 150 °C, however, there is evidence of interdiffusion of Co and Cu, as shown in Fig. 13(a). For a 100 Å Cu film deposited on thick Co at 150 °C, a weak Co *LMM* feature is observed. Similarly, the Co$2p_{3/2}$ feature (not shown) at 476 eV kinetic energy had an integrated intensity almost 2% that of the Cu$2p_{3/2}$ peak at 311 eV, at normal emission. Because the photoelectron cross section of these two features is nearly equal, the ratio of these peak intensities will be roughly equal to the chemical ratio of the two species integrated over the probing depth of the associated photoelectron. Since the mean free path of electrons with energy ~400 eV is about 7 Å,[35] 90% of the XPS signal originates from the outer 16 Å of the sample.

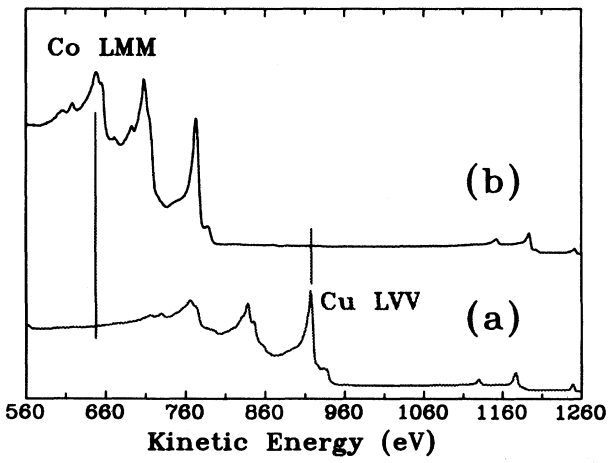

FIG. 12. X-ray-photoelectron energy distribution curves for two samples deposited at 0 °C. Sample (a) consists of 100 Å Cu deposited onto a thick Co film. Sample (b) consists of 100 Å Co deposited onto a thick Cu film. The absence of the Co *LMM* feature in spectrum (a), of the Cu *LVV* feature in spectrum (b) indicate that interdiffusion of Co and Cu does not occur for deposition at 0 °C.

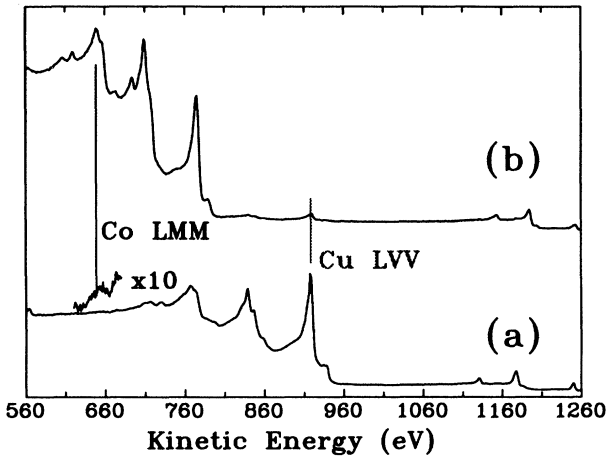

FIG. 13. X-ray-photoelectron energy distribution curves for samples analogous to those of the previous figure, except that they are deposited at 150 °C. Here significant Co-Cu interdiffusion is observed, as evidenced by the presence of the Co *LMM* peak in the thick Cu film (a), and by the presence of the Cu *LVV* peak in the thick Co film (b).

This Co peak was observed to vanish if the XPS spectrum was recorded at a polar angle of 80°. In the latter geometry, the effective mean free path of the electrons is decreased by a factor of 6, so that the XPS is sensitive to only the outermost two monolayers of the sample. From this we conclude that although there is slight interdiffusion of Co into the Cu at 150 °C, this Co is excluded from the outer 2 ML.

Growth of 100 Å of Co onto thick Cu at 150 °C can be analyzed similarly [Fig. 13(b)]. At normal emission, weak features were observed due to Cu near the film surface. The Cu *LVV* Auger peak (918 eV) was measured to be almost 6% as large as the Co *LVV* Auger (773 eV) feature, indicating significant interdiffusion of Cu into the Co layer. In this energy range, the electron mean free path is about 10 Å, and again, the cross sections for excitation of both the Co and Cu features are nearly equal. Interestingly, when the sample is rotated to a polar angle of 80° (for which the sampling depth is about two monolayers) the Cu signal is seen to *increase* by a factor of 2. This supports the model of a higher concentration of Cu in the outer 2 ML of the Co film.

These surface segregation effects agree with intuition, according to the relative surface free energies of Co and Cu. In the case of thick Cu on Co, the Co is excluded from the near surface region because it has a higher surface free energy. However, Co atoms more than 2 ML below the sample surface may be expected to achieve a concentration limited by their bulk solubility in Cu or by the density of grain boundary sites. On the other hand, for thick Co on Cu, the dilute Cu atoms are preferentially driven to the surface by the difference in surface free energies.

To support these data, simple sputter etch depth-

profiling experiments were performed on the two samples deposited at 150 °C. These samples were bombarded with Ar ions so that approximately 2 ML and 4 ML of the surface atoms were removed. Calibrations of the sputter etch rate were determined by etching films of known thickness. These sputter rates agreed well with published data for pure Co and Cu.[36] The Ar ions had a kinetic energy of 3 kV, with a delivered current to a 1-in. diameter sample of $\simeq 200$ nA, at a polar incidence angle of $\simeq 60°$.

The ratios of the Co-to-Cu peak intensities are plotted as a function of etch depth for the two samples in Fig. 14. In Fig. 14(a), the ratio of the Co$2p_{3/2}$ and Cu$2p_{3/2}$ peaks (taken at normal emission) is plotted, for 100 Å of Cu deposited on Co. In Fig. 14(b), the ratio of the Cu *LVV* and Co *LVV* peaks is plotted, for 100 Å of Co deposited on Cu. Note that both curves (a) and (b) show an enhanced Cu concentration in the outer 2 ML. More than 2 ML below the sample surface, the minority species concentrations become constant, as a function of sputter depth. These results agree with the interpretation of the angular dependencies of these features discussed above.

It is interesting to note that the minority impurity concentrations of both Co in Cu and Cu in Co saturate to $\simeq 3\%$, in the bulk of the film. This is consistent with the interpretation that the observed interdiffusion occurs at twin-domain boundaries in the film. Due to the fact that the original Pt buffer layer shows two azimuthal orientations, 180° apart, there is a high percentage of twin boundaries propagated throughout these films. The average grain size in the buffer layer is about 200 Å in diameter.[20] Thus, if a 3% impurity were located only in the boundaries of 200 Å square grains, that impurity region would be $\simeq 1$ ML thick, which is not unreasonable.

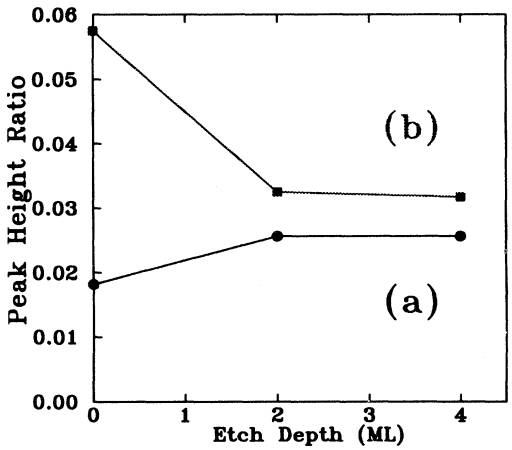

FIG. 14. Results of sputter depth-profiling experiments performed on two samples deposited at 150 °C. Curve (a) is from 100 Å Cu deposited on thick Co. Curve (b) is from 100 Å Co deposited on thick Cu. The plotted values correspond to the peak area ratio of the Co$2p_{3/2}$ and Cu$2p_{3/2}$ photoelectron features (a) and the Cu *LVV* to Co *LVV* Auger electron features (b) as measured at normal emission, for different sputtering times. These sputtering times correspond to the removal of 0, 2, and 4 ML of atoms, as displayed. Note that surface segregation effects cause an increase in the relative concentration of Cu atoms and decrease in the concentration of Co atoms near the surface, in both cases.

Based on these observations, we believe that the majority of the "bulk" impurity atoms seen in these films are localized at grain boundaries caused by twinning. This explains the high concentration of impurities in spite of the fact that Co and Cu are immiscible in the bulk at 150 °C. Furthermore, since impurity atoms are still observed at 100 Å from the Co-Cu film interface, there must be some mechanism for the transport of these impurity atoms over long distances. The most likely channel for such transport, again, must be the grain boundaries. It is therefore not surprising that the impurities are localized to these regions.

These results on thicker films are consistent with our interpretations of XPD on thinner films. If Co-Cu interdiffusion is isolated to the grain boundaries and limited to about 3% impurity levels, this interdiffusion would be below the sensitivity level of the XPD (which is sensitive to interdiffusion on a scale of roughly 20%). Moreover, we have confirmed that Cu surface segregation occurs when both Co and Cu are present near the surface at 150 °C. We find, however, that only ~ 0.1 ML of Cu atoms propagates to the top of 100 Å of Co. This is in contrast with the XPD results on very thin Co films (1–3 ML), for which perhaps 0.5–1 ML of Cu surface segregates.

To summarize the results of the structural characterization, we find that deposition of Co and Cu at 0 °C leads to abrupt Co-Cu interfaces, without interdiffusion. These interfaces are rough, and lead to a rough vacuum interface. At 150 °C, significant Co-Cu bulk interdiffusion occurs, probably mediated by and localized to grain boundaries. In addition, Cu surface segregation occurs when both Co and Cu are present near the surface. Growth at 150 °C leads to a smoother vacuum interface, and to smoother Co-Cu interfaces, possibly due to surfactant properties of the surface segregated Cu.

VII. DISCUSSION

The peak in MR at $\simeq 10$ Å for the Co/Cu(111) wedges agrees well with experiments on sputtered (111)-textured Co/Cu multilayers, although for sputtered films several additional peaks in MR are found with increasing Cu-layer thickness spaced at 10–11 Å intervals. For sputtered films, the positions of these peaks correspond to regions of antiferromagnetic coupling of neighboring Co layers mediated by the Cu spacer layers. The presence of such AF coupling in (111)-oriented single crystalline Co/Cu multilayers has been the subject of some controversy. Although early studies suggested the absence of any such coupling,[7,8] several groups later reported strong, although incomplete, AF coupling.[16–19,15] In each case only a single region of antiferromagnetic coupling was observed, near $t_{Cu} = 10$ Å. Furthermore, the coupling strength in MBE-deposited multilayers is significantly higher than that observed in sputtered multilayers. Both these facts may suggest intrinsic differences in the exchange coupling between epitaxial and sputtered multilayers, and that oscillatory exchange coupling may

not exist in epitaxial Co/Cu (111) multilayers.

Another possible explanation is that subtle defects in the structure lead to ferromagnetic bridges across the Cu layers.[4,19] Since the interlayer magnetic coupling strength is expected to fall off very rapidly with increasing Cu-layer thickness, it would be reasonable that such defects might obscure the AF coupling at all but the first AF coupling peak.

The structural data presented in the preceding section supports this hypothesis. Both grain-boundary diffusion and interface roughness would lead to ferromagnetic coupling of the Co layers. Twin boundary diffusion, which is enhanced at higher growth temperatures, can lead to ferromagnetic coupling directly, with consecutive Co layers communicating directly through Co bridges formed at grain boundaries. Interface roughness causes a variation of the Cu-layer thickness separating Co layers. This can lead to localized regions of ferromagnetic coupling, which may inhibit the measurement of AF coupling.

Another possible explanation for the presence of only a single peak in MR is that this peak has nothing at all to do with Cu-mediated oscillatory AF coupling. Rather, the MR and coupling strength increase *monotonically* with decreasing Cu-layer thickness until a cutoff is reached at small Cu thicknesses. This cutoff is due to widespread direct ferromagnetic bridging across the Cu layers. The antiparallel alignment observed at $\simeq 10$ Å might then be caused by magnetostatic coupling of the Co layers, resulting from the interfacial roughness described above.

The deviations from structural perfection are quite significant. As with the Cu layers, interfacial roughness could lead to variations in the Co layer thickness, especially for samples deposited at 0 °C. For deposition at 150 °C, this roughness is decreased, but there is increased grain-boundary diffusion of Co through the Cu layers. Such structural defects could break up the lateral magnetic coherence of the Co layers, while at the same time establishing magnetic bridges between adjacent Co layers. The three-dimensional magnetic matrix which is formed would tend to behave more like a ferromagnet for very low Cu thicknesses, but have substantial regions of antiparallel alignment of Co domains, separated by Cu, as t_{Cu} is increased. The strength of the interaction causing this antiparallel alignment would then decrease monotonically with increasing t_{Cu}, until for thick Cu layers the Co regions would be decoupled. At this point, the saturation field would be independent of t_{Cu}, and would depend only on the properties of an isolated Co layer. The MR would also follow this behavior, except for small values of t_{Cu}, where the fraction of the sample experiencing antiparallel alignment would rapidly decrease, generating the MR peak at $t_{Cu} = 10$ Å.

Whatever the cause of the initial peak in MR for $t_{Cu} = 10$ Å, the monotonic behavior of MR when $t_{Cu} > 15$ Å can be easily understood based upon the structural measurements. Considering the large interface roughness, we speculate that the magnetic behavior of such Co layers might be more like that of Co particles suspended in a Cu matrix, especially for thick Cu interlayers. The behavior of Co particles in a Cu matrix (known as a granular alloy) has recently received considerable attention,[37–39] since such structures show large MR. This MR varies smoothly with Cu concentration, and requires large saturation fields (maximum $\simeq 40$ kOe). This behavior is very similar to what is observed here, as large MR is obtained in the multilayers which varies smoothly with Cu-layer thickness, and requires large saturation fields ($\simeq 20$ kOe) which also vary little with Cu-layer thickness.

One interesting point is that the MR maximum observed at $t_{Cu} \simeq 10$ Å is 25% higher for samples deposited at 150 °C relative to 0 °C. At the same time, magnetization measurements (Fig. 4) show a nearly equal proportion of AF coupled to ferromagnetically coupled regions in both samples. Thus, the net MR for a given AF-coupled region appears to be higher for growth at 150 °C. This is correlated with the observed smoothing of the film interfaces at the higher temperature. This correlation is exactly the opposite to what has been reported for Fe/Cr multilayer films deposited by magnetron sputtering.[40] One explanation of these contradictory results is that there is an *optimal* roughness scale, for the maximization of MR. Thus, if one begins with relatively smooth films, roughening improves the MR. But if one deposits films with a larger interlayer roughness, as here, smoothing causes an increase in MR.

VIII. CONCLUSIONS

We have studied the deposition temperature dependence of magnetic properties and growth morphology for Co/Cu SL's along the [111] orientation, using magnetoresistance, magnetization, x-ray-photoelectron diffraction, x-ray-photoelectron spectroscopy, and x-ray diffraction. Samples were prepared as superlattice wedges, which allows for the preparation of a large number of samples with different film thicknesses under identical growth conditions.

At all the temperatures studied (0, 150, 200 °C), we find evidence for only one peak in MR as a function of Cu-layer thickness at $t_{Cu} \simeq 10$ Å. We find that the 4.2-K MR of samples deposited at higher temperature is greater than that for SL's deposited at 0 °C, in the range $t_{Cu} \simeq 6$–15 Å, and lower in the range $t_{Cu} \gtrsim 15$ Å. All samples displayed a perpendicular magnetic anisotropy, and very large saturation fields. The saturation field was seen to decrease from $\simeq 60$ kOe for $t_{Cu} \simeq 7$ Å to $\simeq 20$ kOe for $t_{Cu} = 15$ Å, beyond which it remained approximately constant for $t_{Cu} > 15$ Å.

Growth mode studies concentrated on samples deposited at 0 and 150 °C. XPD measurements were used to determine the growth mode of Co on Cu in the low thickness regime. At 0 °C, diffusion-limited layer-by-layer growth is observed. This means that some fraction of the $(n+1)$th terraces form before the nth layer is complete. This roughness accumulates as the SL is deposited and leads to a rough vacuum interface when the SL is complete (as determined by XRD). At 150 °C, ≤ 1 ML of Cu atoms surface segregate at all stages of Co film growth. Increased diffusivity of the Co atoms, and a possible surfactant effect of the Cu monolayer, causes flatter Co films leading to a smoother vacuum interface when the SL is

complete (as determined by XRD).

X-ray-photoelectron spectroscopy measurements and sputter etch depth-profiling experiments were used to probe the growth modes for film thickness $\simeq 100$ Å. For 0 °C growth, no long-range interdiffusion was observed for either Co on Cu, or Cu on Co. At 150 °C, some interdiffusion was observed, leading to approximately 3% bulk impurity concentrations for both Co in Cu, and Cu in Co. Because such impurity concentrations are not expected according to the bulk phase diagram, we believe that impurity diffusion is both localized to, and mediated by grain boundaries present in these films due to twinning of the original Pt buffer layer on sapphire. Surface segregation of Cu was observed for both Cu-rich and Co-rich films.

For $t_{Cu} < 15$ Å, the smoothing of the films at 150 °C appears to lead to increased MR, relative to films deposited at 0 °C. But due to the excessive roughness present in all films, MR peaks at higher Cu-layer thickness are unobservable, if such peaks exist. In fact, for $t_{Cu} > 15$ Å, the SL's behave similar to Co-Cu granular alloys,[37–39] showing large MR and saturation fields, with only weak dependence on the amount of Cu deposited.

ACKNOWLEDGMENTS

The authors gratefully acknowledge H. Notarys and J. C. Scott for the ellipsometry measurement of the thick Cu layer on glass, T. Suzuki for assistance with the alternating gradient magnetometry measurements, and K. P. Roche for technical support.

[1]G. Binasch, P. Grünberg, F. Saurnbach, and W. Zinn, Phys. Rev. B **39**, 4828 (1989).
[2]M. N. Baibich *et al.*, Phys. Rev. Lett. **61**, 2472 (1988).
[3]S. S. P. Parkin, N. More, and K. P. Roche, Phys. Rev. Lett. **64**, 2304 (1990).
[4]S. S. P. Parkin, R. Bhadra, and K. P. Roche, Phys. Rev. Lett. **66**, 2152 (1991).
[5]S. S. P. Parkin, Z. G. Li, and D. J. Smith, Appl. Phys. Lett. **58**, 2710 (1991).
[6]S. S. P. Parkin, Phys. Rev. Lett. **67**, 3598 (1991).
[7]W. F. Egelhoff, Jr. and M. T. Kief, Phys. Rev. B **45**, 7795 (1992).
[8]R. F. Marks, R. F. C. Farrow, S. S. P. Parkin, C. H. Lee, B. D. Hermsmeier, C. J. Chien, and S. B. Hagstrom, in *Heteroepitaxy of Dissimilar Materials,* edited by R. F. C. Farrow, J. P. Harbison, P. S. Peercy, and A. Zangwill, MRS Symposia Proceedings No. 221 (Materials Research Society, Pittsburgh, 1991), p. 15.
[9]A. Schreyer, N. Metoki, Th. Zeidler, P. Bödeker, A. Abromeit, Ch. Morawe, U. Romahn, P. Sonntag, K. Bröhl, and H. Zabel, J. Magn. Magn. Mater. (to be published).
[10]A. Cebollada, J. L. Martinez, J. M. Gallego, J. J. de Miguel, R. Miranda, S. Ferrer, F. Batallan, G. Fillion, and J. P. Rebouillat, Phys. Rev. B **39**, 9726 (1989).
[11]A. Cebollada, R. Miranda, C. M. Schneider, P. Schuster, J. Kirschner, J. Magn. Magn. Mater. **102**, 25 (1991).
[12]F. Giron, P. Boher, Ph. Houdy, F. Pierre, P. Beauvillian, C. Chappert, K. Le Dang, and P. Veillet (unpublished).
[13]M. T. Johnson, S. T. Purcell, N. W. E. McGee, R. Coehoorn, J. ann de Stegge, and W. Hoving, Phys. Rev. Lett. **68**, 2688 (1992).
[14]B. Heinrich, J. F. Cochran, M. Kowalewski, J. Kirschner, Z. Celinski, A. S. Arrott, and K. Myrtle, Phys. Rev. B **44**, 9348 (1991).
[15]M. T. Johnson, R. Coehoorn, J. J. de Vries, N. W. E. McGee, J. ann de Stegge, and P. J. H. Bloemen, Phys. Rev. Lett. **69**, 969 (1992).
[16]J. P. Renard, P. Beauvillian, C. Dupas, K. Le Dang, P. Veillet, E. Vélu, C. Marliére, and D. Renard, J. Magn. Magn. Mater. **115**, L147 (1992).
[17]J. Kohlhepp, S. Cordes, H. J. Elmers, and U. Gradmann (unpublished).
[18]D. Greig, M. J. Hall, C. Hammond, B. J. Hickey, H. P. Ho, M. A. Howson, M. J. Walker, N. Wiser, and D. G. Wright, J. Magn. Magn. Mater. (to be published).
[19]S. S. P. Parkin, R. F. Marks, R. F. C. Farrow, Q. H. Lam, G. R. Harp, and R. J. Savoy, Phys. Rev. B **46**, 9262 (1992).
[20]R. F. C. Farrow, G. R. Harp, R. F. Marks, B. Hermsmeier, M. F. Toney, T. A. Rabedeau, and S. S. P Parkin (unpublished).
[21]The scattering vector is the difference between the incoming and scattered x rays and has a magnitude $Q=(4\pi/\lambda)\sin[(2\theta)/2]$. In the specular scans $Q=Q_z$, the component of the scattering vector perpendicular to the substrate surface.
[22]In the off-specular scans $Q_z=Q\cos\{[(2\theta)/2]-\theta\}\simeq Q$ and the component of the scattering vector parallel to the substrate surface is $Q_x=Q\sin\{[(2\theta)/2]-\theta\}$. For the data shown in Fig. 8(b), Q_x varies between 0.0003 and 0.0015 Å^{-1}.
[23]M. F. Toney and C. Thompson, J. Chem. Phys. **2**, 3781 (1990).
[24]T. A. Rabedeau *et al.* (unpublished).
[25]L. Z. Mezey and J. Giber, Jpn. J. Appl. Phys. **21**, 1569 (1982).
[26]Specifically, the bulk solubility at 422 °C for Cu in Co is 0.4% [*Binary Phase Diagrams,* 2nd ed. edited by T. B. Massalski (ASM International, CITY, 1990), Vol. 2, p. 1189]. Below 500 °C the bulk solubility of Co in Cu less than 0.1% [M. Hansen, *Constitution of Binary Alloys* (McGraw-Hill, New York, 1958), p. 469].
[27]Q. Chen, M. Onellion, and A. Wall, Thin Solid Films **196**, 103 (1991).
[28]For a review of photoelectron diffraction, see C. S. Fadley, in *Synchroton Radiation Research: Advances in Surface Science,* edited by R. Z. Bachrach (Plenum, New York, 1990).
[29]M. Copel, M. C. Reuter, Efthimios Kaxiras, and R. M. Tromp, Phys. Rev. Lett. **63**, 632 (1989).
[30]M. Horn-von Hoegen, F. K. LeGoues, M. Copel, C. Reuter, and R. M. Tromp, Phys. Rev. Lett. **67**, 1130 (1991).
[31]S. D. Bader and E. R. Moog, J. Appl. Phys. **61**, 3729 (1987).
[32]F. J. Himpsel, Phys. Rev. B **44**, 5966 (1991).
[33]H. Li and B. P. Tonner, Surf. Sci. **237**, 141 (1990).
[34]G. J. Mankey, M. T. Kief, and R. F. Willis, J. Vac. Sci. Tech. (to be published).
[35]M. P. Seah and W. A. Dench, Surf. and Inter. Anal. **1**, 2 (1979).
[36]H. H. Andersen and H. L. Bay, in *Sputtering by Particle Bombardment* I, edited by R. Behrisch, Topics in Applied Physics

Vol. 47 (Springer-Verlag, Berlin, 1981).
[37]A. E. Berkowitz, J. R. Mitchell, M. J. Carey, A. P. Young, S. Zhang, F. E. Spada, F. T. Parker, A. Hutten, and G. Thomas, Phys. Rev. Lett. **68**, 3749 (1992).
[38]J. Q. Xiao, J. S. Jiang, and C. L. Chien, Phys. Rev. Lett. **68**, 3749 (1992).
[39]S. S. P. Parkin, R. F. C. Farrow, T. A. Rabedeau, R. F. Marks, G. R. Harp, Q. H. Lam, C. Chappert, M. Toney, R. Savoy, and R. Geiss, Europhys. Lett. (to be published).
[40]E. E. Fullerton, D. M. Kelly, J. Guimpel, and Ivan K. Schuller, Phys. Rev. Lett. **68**, 859 (1992).